Marine Pollution Bulletin 191 (2023) 114958

Contents lists available at ScienceDirect

Marine Pollution Bulletin

journal homepage: www.elsevier.com/locate/marpolbul

Aerial remote sensing of sub-sea dispersant injection effects during the Deepwater Horizon (MC-252) oil spill

Jan Svejkovsky [a,*], Mark Hess [b], Judd Muskat [c], James White [b]

[a] Ocean Imaging Corp., 13976 West Bowles Ave, Suite 100, Littleton, CO 80127, USA
[b] Ocean Imaging Corporation, Littleton, CO, USA
[c] Office of Spill Prevention and Response, California Dept. of Fish and Wildlife, Sacramento, CA, USA

ARTICLE INFO

Keywords:
Oil spill
Subsea dispersants
Deepwater Horizon
Remote sensing
Surfacing oil

ABSTRACT

During the Deepwater Horizon oil spill in 2010, subsea dispersant injection (SSDI) was utilized for the first time in an effort to reduce the amount of oil reaching the sea surface and thus potentially decrease its environmental impact and enhance responders' safety. Since then, controversy has developed about SSDI's effectiveness. Most of the analysis is based on modeling, with some models concluding SSDI significantly reduced surfacing oil volumes, and others predicting that processes unrelated to the dispersant caused most of the subsurface oil retention. This study utilized a multispectral aerial sensor image time series to correlate the surface area covered by freshly upwelled oil with changes in SSDI rates, accounting for an approximate 4 hour oil rise time lag. A significant negative correlation was found between oil-covered surface area and SSDI rates, providing direct observation support that the technique did reduce the amount of surfacing oil around the wellhead.

1. Introduction

On 20 April 2010 the Deepwater Horizon (DWH) oil rig exploded in the Gulf of Mexico and continued to spill oil into the sea until 15 July 2010 when the wellhead was finally capped. The spill was the largest in the US, and second largest in history, exceeded only by the Mina al Ahmadi spill during the first Gulf War in 1991. As part of the response, several novel technologies were utilized. These included the first-ever injection of chemical dispersants at the wellhead, approximately 1500 m below the surface. Corexit™ 9500 – the primary dispersant utilized during the incident – is composed of surfactants that act to lower the interfacial tension between the oil and water, which allowed turbulence from the release to create small oil droplets that only slowly rose to the surface (Brandvik et al., 2018). This causes longer oil retention in the water column resulting in increased oil dissolution and biodegradation, and thus less oil and volatile organic compounds (VOCs) actually surfacing, especially in the vicinity of well-control operations, hence increasing the efficiency and safety of response efforts above the spill location. Such effects have been successfully modeled (Socolofsky et al., 2015; Spaulding et al., 2017; Gros et al., 2017), and the Corexit™ 9500-caused changes in oil droplet size underwater have been experimentally observed (Aprin et al., 2015; Brandvik et al., 2013; Johansen et al., 2013). MacDonald et al. (2015) used Synthetic Aperture Radar (SAR) satellite data to estimate the volume of floating oil throughout the spill event, and found a 21 % decrease between late May and mid-June. They attributed the decrease to "increased applications of dispersant and surface burning operations". However, in the years following the incident, some members of the research community began expressing doubts that the massive subsea dispersant injection (SSDI) efforts had major effects. They believe natural oil dispersion caused by turbulent mixing induced by the pressurized discharge of hot oil and gas into entrained cold seawater had the same effect as dispersants (Peterson et al., 2012). Aman et al. (2015) and Malone et al. (2018) conducted experiments with methane-saturated oil in a high-pressure autoclave (to simulate conditions present in a deep water blowout) and concluded that the dissolved methane and subsequent pressure changes caused the "live" (gas-saturated) oil to atomize into microdroplets in the absence of any dispersants. Paris et al. (2018) used a subsurface water chemistry sample archive collected throughout the incident to also claim that the dispersant injections caused no significant oil distribution changes both vertically and at the surface. More recently, however, Zhao et al. (2021) used over 90,000 air measurements collected on 20 vessel decks located within 2 miles (3.7 km) of the Macondo well during the DWH incident to demonstrate with a high level of statistical confidence that SSDI reduced

* Corresponding author.
E-mail address: jan@oceani.com (J. Svejkovsky).

https://doi.org/10.1016/j.marpolbul.2023.114958
Received 28 February 2023; Received in revised form 4 April 2023; Accepted 14 April 2023

airborne VOC concentrations in a dose-dependent manner to protect response workers on these vessels.

Another novel technology utilized during the DWH spill was the near-real-time generation and dissemination of surface oil thickness maps derived from an aerial multispectral sensor flown by Ocean Imaging Corp. (OI) nearly daily. Since the overall spill very soon became too large to be imaged by this sensor in its entirety, the daily missions were tasked by the Unified Command to image specific regions, ranging from the spill source area, to outer extents of the spill, to nearshore and shoreline sections (Svejkovsky et al., 2012). Because the spill source site was of primary, continued interest, it was imaged most frequently. An example OI analysis from the response is shown in Fig. 1. The very high resolution (2 m) imagery offered a new tool to directly observe any changes related to surfacing oil intensity over the spill source site. During the major SSDI test on May 10–11, 2010, multiple imaging missions were undertaken to document the surface oiling extents before, during and after the tests. The imagery and resulting oil thickness pattern characterizations were part of data provided to the U.S. Environmental Protection Agency for assessment on whether to allow continued use of the SSDI technique. Qualitative assessment of the images as well as oil thickness characterizations showed a marked apparent decrease in the thickest oil classes around the spill source site during the active injection period, then a notable increase in thick oil surface coverage after the injection was stopped (Svejkovsky and Hess, 2012).

A more comprehensive assessment of the spill source area surface oiling patterns as they related to variations in the SSDI rate was included in Svejkovsky et al.'s (2016) analysis of aerial and satellite imagery throughout the entire spill period: total area of fresh oil thicker than 16 μm within a 7 km radius around the source location was compared with daily volumes of dispersant injected. The data showed that days with the largest thick oil coverage corresponded to days when no dispersant was injected subsea (early to mid-May 2010). Conversely, the smallest thick oil coverage area generally corresponded to days when >10,000 gal/day of dispersant were injected subsea. The past investigation was not, however, focused on the SSDI effectiveness question, and the relationship was not specifically quantified. In this paper we present results of a detailed investigation targeting the potential relationship between DWH spill source area surface oil manifestations (as derived from the existing aerial imagery) and applicable (i.e. time-lag-adjusted) SSDI rates. Our results suggest that there was indeed a relation between the time-variability in SSDI rates and the variability of oil amounts on the ocean surface in the immediate DWH spill source area, providing unique direct imaging-based support for the SSDI's effectiveness.

2. Materials and methods

2.1. Study area

The study area for this analysis was a 2 nautical mile (3.7 km) radius around the Macondo-well location. We chose this area because it contained the primary well-response vessels. There were up to 20 vessels working within 2 nautical miles of the well from early May to late July 2010. These vessels housed over 1000 response workers during this period (Zhao et al., 2021). We focused our analysis on this area in order to determine if SSDI reduced oil surfacing there, and thereby protected response workers from volatiles emanating from fresh oil.

2.2. Aerial imagery

During the DWH event, OI utilized its Digital Multispectral Camera (DMSC-MkII) imager manufactured by SpecTerra Ltd. in Australia. This frame-grabber type imager used four lenses and 41,024 × 1024 silicon-based CCDs to yield four data channels with 12-bit radiometric resolution. Each channel's wavelength range was customized with 10 nm-wide interference filters. Based on previous research, the system was configured with three channels in the visible and one in the near-IR (450, 551, 600 and 710 nm). The DMSC was coupled with a Jenoptik IR-TCM-640 (640 × 480) camera, providing one channel in the thermal-IR (see Table 1 for further specifications). Both imagers were integrated with an Oxford Technologies 2502 DGPS/IMU positioner with 100 MHz update rate and 2 m circular positioning error under Space Based Augmentation System (SBAS) conditions. OI's custom software was used to auto-georeference and mosaic the acquired image frames. Previous tests with this system configuration and software showed RMS positioning error after the auto mosaicking of <6 m at 3040 m flight altitude (Svejkovsky and Muskat, 2009).

Under direction from the National Oceanographic and Atmospheric Administration (NOAA) and BP, OI was mobilized to aid the DWH Spill response on 1 May 2010. Following equipment installation on-board a NOAA Twin Otter aircraft, the oil mapping system was first utilized on 4 May 2010. In the following days, until 26 July 2010, the OI imaging and NOAA aircraft teams flew 1 to 2 imaging missions almost daily, based out of Mobile, Alabama. Since sunglint severely degraded image usefulness of visible wavelength imagery from the DMSC sensor, imaging was limited to several hours in the morning after sunrise and several hours in the afternoon before sunset when low sun angles prevailed. (The thermal IR imagery is not affected by sunglint and could be used throughout the day and night.) In the offshore regions the system was flown at 3800 m altitude, yielding 2 m multispectral and 4 m thermal-IR resolution imagery.

2.3. Oil thickness classification and adaptation to DWH conditions

OI had previously developed an oil film thickness determination algorithm utilizing image data from the DMSC/IR system. This algorithm was developed and validated over several years utilizing controlled experiments at the Bureau of Safety and Environmental Enforcement's outdoor Ohmsett facility in New Jersey, as well as field experiments utilizing natural oil seeps in Santa Barbara Channel, California (Svejkovsky and Muskat, 2006; Svejkovsky et al., 2008; Svejkovsky and Muskat, 2009). The system was first used experimentally during the 2007 *M/V Cosco Busan* spill in San Francisco Bay, and then operationally during several spills in California such as the Platform A spill in 2008 (Svejkovsky et al., 2009).

The developed oil thickness mapping procedure consists of two steps: The first step utilizes a neural network classification algorithm applied to the four available DMSC channels to identify all imaged ocean surface areas that likely contain some oil, and to eliminate artifacts caused by sunglint (the most common), high suspended sediment, floating kelp, and seaweeds, etc. The second step, specifically targeting thickness distributions, is then applied only to the pixels believed to contain oil. For each oil-contaminated pixel, it utilizes the deviation of the different available band ratios from the "clear water ratios" (computed in neighboring areas with no oil contamination or, in the DWH case, water covered by sheens invisible to the eye). The objective is to utilize the ratio deviations from site and time-specific background reflectance (rather than absolute ratio values as was done in previously published studies by others) to better account for regional differences in water color, temperature, and illumination characteristics.

During the DWH response OI utilized its thickness algorithm to delineate five thickness range classes. They were: Sheen/Thin Oil (<0.008–0.015 mm); Mid-thick Oil (0.016–0.08 mm); Thick Fresh Oil (0.09–0.2 mm), Thickest Fresh Oil (>0.2 mm), and Emulsified Oil (any thickness). The Thickest Fresh Oil class was primarily based on the thermal channel showing a positive thermal contrast relative to surrounding water, as was observed during extensive previous controlled research (Svejkovsky et al., 2012).

2.4. Data processing for SSDI rate vs. surface oil comparisons

Between OI's first imaging mission on 5/4/2010 and 7/15/2010

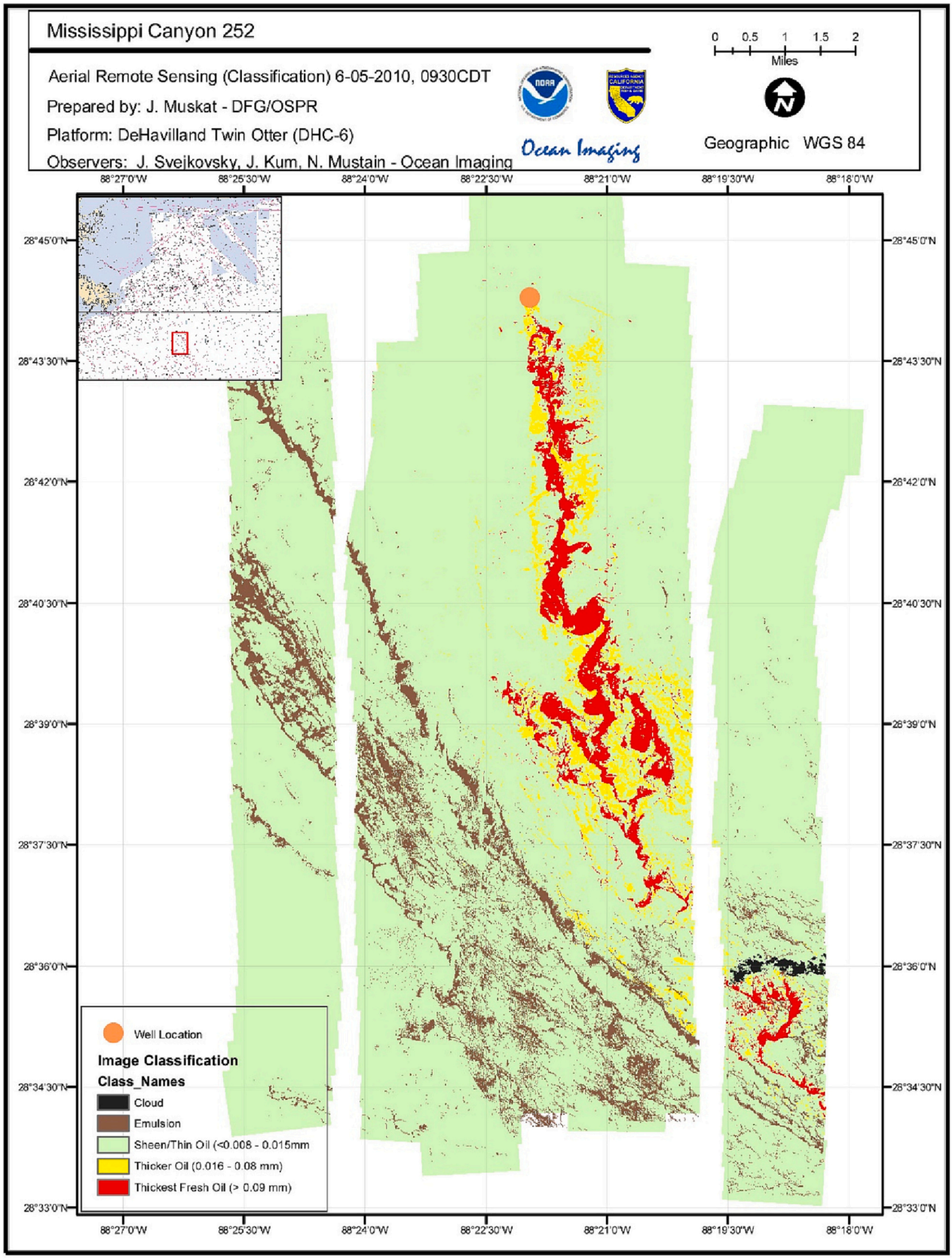

Fig. 1. Oil thickness pattern analysis of the DWH spill source region generated by Ocean Imaging Corp. on 6 May 2010.

Table 1
Specifications of imaging instruments utilized by OI during the DWH spill.

	DMSC Mk-II	Jenoptik IR-TCM640
Detector type	Progressive-scan CCD	Uncooled Microbolometer
Number of channels	4 customizable w/ 10 nm interference filters	1
Image format	1024 × 1024 pixels	640 × 480 pixels
Spectral range	400–950 nm	7.5–14 μm
Dynamic range	12-bit	16-bit
Thermal resolution		<70mK
Field of view	29.3° × 29.3°	30° × 23°
Dimensions	25.4 cm × 25.4 cm × 27 cm	153 cm × 91 cm × 111 cm
Weight	16.3 kg	1.05 kg

when the wellhead was permanently capped, 46 image data sets included coverage of several kilometers over and around the DWH spill source site. As was already noted, however, with the usual additional multiple target region assignments and sunglint-restricted time window, the time spent imaging the source area was limited. The prime objective at the time was to document the direction, overall expanse and thickness characteristics of the oil plume rather than to create a seamless map over a set area. Therefore, on some days progressive flight lines were purposely offset with small data gaps between them to increase overall spatial coverage, or flight lines were terminated early on the opposite side of the plume direction where no oil or only sheen existed. For purposes of this study, we deemed it necessary to have at least 90 % complete image coverage within the study area on a given flight regardless of plume direction and extent. We were able to identify 33 data sets satisfying this criterion at 2 nautical miles (3.7 km) radius around the spill source location (the simultaneous operations (SIMOPS) radius was 2.5 nm). Assuming usual surface drift rates between 10 cm/s and 50 cm/s, the study area thus contained a 2.0–10.3 h-long record of oil after it reached the surface. This time interval would be somewhat shortened on days when the apex of the plume was displaced up to several hundred meters from the seabed release location, likely due to subsurface currents (Svejkovsky et al., 2016). By far the largest horizontal displacement of the plume from the spill source location was observed on 5/23/2010 (1.66 km) and that data set was excluded from the study (Fig. 4). The original data from the selected image sets were carefully re-mosaicked, quality checked for geolocation accuracy (using permanently stationed rigs near the source as reference points), and reprocessed for thickness with the original algorithm. For this study the two thickest oil classes used during the DWH response were combined. The oil thickness analyses were then used to compute the total area within the 3.7 km radius circle covered by the thickest fresh oil classes (≥0.016 mm) in each image set. Emulsified oil features were not included in the thick oil area since they are believed to represent aged floating oil that was advected back into the immediate spill source region. Table 2. lists the thickness classification class characteristics.

The SSDI data were obtained from two sources. The first contains daily average values (based on UTC time) for May and most of July 2010 (Gulf Stream Initiative, 2018). Between 6/2/2010 and 7/4/2010, however, hourly injection rates are available from a NOAA data base (NOAA, 2015). This data set also includes notes on any SSDI stoppages on a minute by minute basis. Fig. 2 shows the SSDI data set and the corresponding dates of the 33 image sets used for analysis. The combined SSDI data set is the most detailed that we found available for this study and was previously utilized in a study of offshore responders' exposure to VOCs (Zhao et al., 2021).

Table 2
Oil thickness class characteristics.

Thickness class	Thickness range in mm	Used for analysis
Thickest Fresh Oil	≥0.09	Yes
Thicker Fresh Oil	0.016–0.08	Yes
Thin Fresh Oil	0.008–0.15	No
Emulsions	Any thickness	No

The hourly data indicate a very significant intraday variability in the injection rate, which could have an important effect on relating the SSDI rates to the few hours' record of surfaced oil. It is reasonable to assume that the great intraday variability also existed during the time periods for which only daily averages are available. Additionally, the vertical travel time lag between when the oil exited the well (and dispersant was applied) and when it reached the surface must be considered. The rise of oil droplets from a deep water blowout differs from blowouts in shallower depths, in that it encompasses multiple phases. Due to the ambient density gradient in the ocean, the initial plume containing a mixture of oil, gas and entrained ambient sea water is arrested as it rises through the water column, and one or more intrusion layers form. Oil droplets then escape the intrusion layers and rise as Lagrangian particles (Socolofsky et al., 2015; Johansen, 2003). In the DWH case, dominant intrusions were observed centered on 1100 m and 800 m depths (Socolofsky et al., 2011; Spier et al., 2013). Ryerson et al. (2012) reported that visual observations from response vessels at the DWH source site suggested a ~3-hour lag time between deliberate intervention at the well and the onset of change in the fresh surface slick. This time corresponds to a mean buoyant velocity of 0.14 m/s from 1500 m depth. It is generally consistent with rise rates observed during the DeepSpill experiments following an intentional release of gas and oil from 844 m depth off Norway (Johansen et al., 2003). The time lag must be considered in the linking of SSDI rates and any changes in surfacing oil amounts detected by the aerial imaging. Considering these previous observation ranges and surface drift estimates, we chose to utilize for analysis the average SSDI rate computed over an 8 hour interval ending 4 h prior to the aerial imaging time. This time period encompasses most closely the time interval of surfaced oil residing within the study area at time of imaging. On days with hourly rates available, the mean rate was computed directly. For days with only daily values available but the 8-hour interval spanning 2 dates (accounting for UTC time), the two daily averages were used, weighted by the number of hours applied from each day.

3. Results

Modeling results indicate that oil droplets released from the well and not affected by contact with dispersant would have the largest size (up to several mm), would rise the fastest through the water column, and would thus surface closest to the wellhead location. French-McCay et al. (2021) computed a 0.7 mm droplet to surface 4.3 km from the well assuming a vertically averaged, unidirectional current of ~7 cm/s. Gros et al. (2017) predicted that with dispersant injection, 98 % of the oil contributing to surface slicks arrived at the sea surface within a 1.0 km^2 area that spanned a horizontal distance of 0.1–2.1 km from the release location under conditions existing on 8 June 2010. Our hypothesis to be tested was that intervals with no dispersant or relatively low SSDI rates would result in larger accumulations of thicker fresh oil after it rose to the surface in the immediate vicinity (3.7 km radius) of the spill source. Conversely, relatively high SSDI rates would correlate to a decreased surfaced thick oil manifestation above the source location. On days when a definite oil plume existed, our imaging observations showed its apex to be located 0.0–1.66 km from the release location. On other days the fresh oil areas were more disorganized and covered or bordered the release location in multiple directions.

Computing the Pearson Correlation Coefficient (r) for the 33 SDDI rate / thick fresh oil area pairs yields a value of −0.51, which is solidly significant at the 0.01 significance level. The data are graphed in Fig. 3, which also highlights an apparent outlier: on 5/6/2010 no dispersant was being injected, yet the image analysis yields relatively little area (6.5 %) covered by thick fresh oil within the 3.7 km radius around the

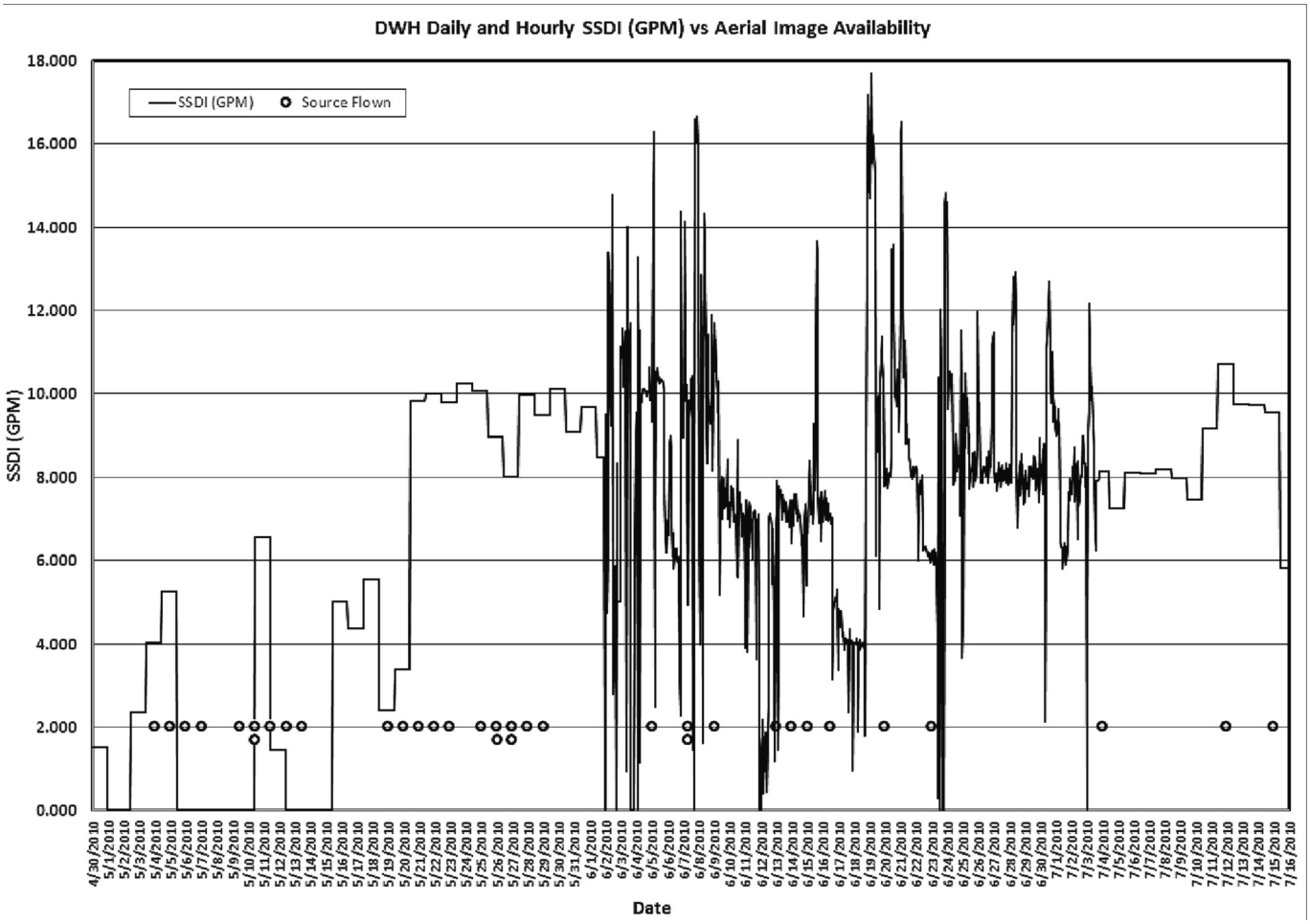

Fig. 2. Subsea dispersant injection rates as daily and hourly (2nd June–4th July) averages in gallons per minute. The dots show dates of aerial imaging sets used for the analysis. Double dots indicate both am and pm flights were conducted.

spill source. Examination of the imagery and oil thickness distribution analysis (Fig. 1) reveals that on that day the oil plume was confined to an unusually narrow but quite long southward-directed plume. This was not observed on other days, since during times when the fresh plume had a distinct directionality, it tended to assume a triangular shape – expanding in width with distance (Fig. 4). Interestingly, winds were light (<2 m/s) throughout the day, and the apex of the plume was located near-directly over the source location, indicating light subsurface currents. Examination of a sequence of sea surface temperature images from NOAA satellites' Advanced Very High Resolution Radiometer suggests a narrow southward-directed convergence zone may have existed south of the well location on 5/6/2010, which could have aggregated the surfaced oil and pushed it southward away from the well location. If this sample set is removed from the data, r increases to −0.61. Both options support the hypothesis that increased SSDI rates did reduce the amount of surfaced oil in the immediate source area.

Data related to the initial May 10–11 dispersant release test provide especially clear visual and quantitative evidence of changes in thick oil surface coverage above the well related to the dispersant injection. Unlike later on in the response when some volume of dispersant continued to be injected most of the time, the May test was preceded by several days of no dispersant injection, and followed by several no injection days, making it a true off-on-off event. Fig. 5 shows SLR photos and corresponding DMSC-derived oil thickness classifications during the event. Data collected on May 9th (not shown) showed that 24.73 % of the 2 nm radius area was covered by the two thick oil classes (≥0.016 mm). A May 10th am overflight, approximately 4–4.5 h after the injection began (it took approximately 30 min to cover the area with overlapping flightlines) resulted in 12.76 % of the area being covered by thick oil. Taking the anticipated oil rise time into account, the study area likely contained oil signatures that surfaced before the injection start but did not yet drift out of its perimeter. The May 10th pm survey, done approximately 13–13.5 h after the injection start (i.e., just past the midpoint of the test) shows a dramatic reduction in heavy surface oiling (1.47 % of area is covered in thick oil) which is also evident in the SLR photo. The next survey was done on May 11th pm, approximately 5–5.5 h after injection was stopped and shows increased heavy oil surfacing (18.47 %), followed by an increase to 34.46 % on May 12th am, and 46.38 % on May 13th am (not shown) with no injection.

4. Discussion and conclusions

Our results indicate that, when a time-lag due to the rising of oil droplets from 1500 m is accounted for, there was a significant negative correlation between the SSDI rate and the amount of freshly surfaced oil in the immediate vicinity of the well location. The greatest surface oil amounts were observed in early May on days when no dispersant was being injected. Similarly high oiling amounts were also observed on 6/7/2010 am (16 % of study area covered), 6/7/2010 pm (23.5 %), and 6/9/2010 am (33.7 %). The Top Hat operation was in-place at that time and the time-lagged 8-hour average injection rates were 8.7–9.7 GPM, a relatively high rate. The original high temporal resolution injection log from that time period (NOAA, 2015) may help explain the apparent weak correlation on those days: the log lists 4 SSDI shut-downs

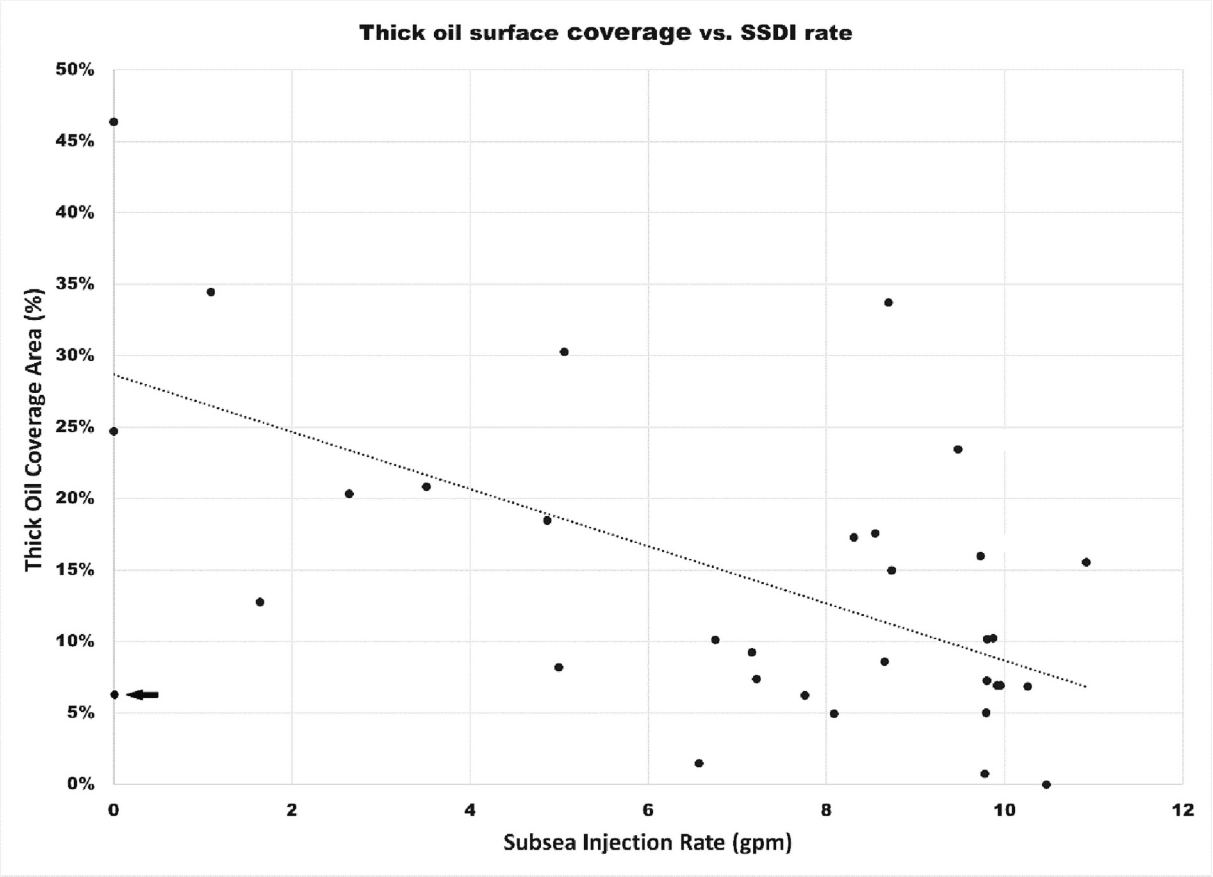

Fig. 3. 8-Hour time-lagged average (see text) subsea injection rates and corresponding "thick oil" (>0.016 mm) sea surface area coverage. The coverage is represented as percent of area within a 2 nautical mile (3.7 km) radius circle centered on the wellhead. Arrow shows potential outlier shown in Fig. 1 and discussed in the text.

throughout the day on 6/7/2010, with the shortest lasting 25 min and the longest 87 min, for a total of 3.5 h when no dispersant was affecting the discharging oil. Similarly, on 6/8/2010 the injections were stopped six times throughout the day for a total of 3 h (the stoppages would be expected to affect oil accumulations in the 6/9/2010 am imagery). Reasons noted for the shutdowns range from maintenance issues to "high benzene levels and VOCs". Upon resumption of pumping, the rates listed are often very high – 14–16 GPM – which acted to increase the computed 8-hour rate averages. Obviously, the higher rates had no effect on oil that escaped the well in the preceding shut-down periods. We thus propose that days with frequent, lengthy SSDI shut-downs likely resulted in larger quantities of oil surfacing in the SIMOPS zone, despite potentially high recorded daily-average injection rates. The injection log lists even more and longer stoppages on 6/12/2010, but no OI imagery was collected over the well site on that day or the next. Several days when imagery was available logged shorter periods of SSDI stoppage, some of which occurred outside the 8-hour average rate computation window. We note that to preserve data consistency, none of the days with known SSDI gaps were removed from the correlation analysis, since it is unknown which other days experienced stoppages during the time series intervals when only daily SSDI rates were available.

The spatial patterns of freshly surfaced oil recorded in the imagery generally agree with model predictions that assumed either a unimodal droplet size distribution with median oil droplet diameter > 1 mm (Socolofsky et al., 2015; Gros et al., 2017), or a bimodal droplet size distribution that included both microdroplets and >1 mm droplets (Spaulding et al., 2017; French-McCay et al., 2021).The models predict that the oil fraction composed of the largest particles not affected by dispersant surfaced within 2 km of the wellhead. Our observations of repeated surfacing of fresh oil in close proximity to the well location (both without and with active SSDI) do not support results of models assuming that most or all of the released oil was in naturally-created microdroplets (<130 μm diameter) regardless of dispersant injection. Such modeling results predicted that no oil or only minimal amounts surfaced near the wellhead (Paris et al., 2012; Aman et al., 2015; Lindo-Atichati et al., 2016; Bracco et al., 2020), which was clearly not the case.

Both French-McCay et al. (2021) and Gros et al. (2017) calculate that the SSDI applications reduced the VOC content of the surfacing oil in the SIMOPS zone by 26–28 % after Top Hat was installed on 6/4/2010. Zhao et al. (2021) showed VOCs were significantly reduced by the SSDI applications using ship-based and personal VOC recorder data. Their data show isolated spikes on 6/7–8/2010, the same time interval discussed above that was plagued by SSDI shutdowns and showed unexpectedly large areas of thick fresh oil in our SIMOPS study area. This suggests that the aerial image analyses may provide useful supplemental data for the assessment of VOC exposures, and provides further support for the argument that SSDI did significantly reduce the amount of oil surfacing around the DWH wellhead.

Several events occurring during the spill response timeline may have temporarily or permanently altered the volume of oil reaching the sea surface. Most notable of these was Operation Top Hat 4 on 6/4/2010: the collapsed riser pipe was cut, creating a single major oil outlet (vs. 3 outlets prior), and a concrete dome was placed over the riser. The dome contained a pipe to the surface through which some of the oil and gas began to be recovered directly. The new configuration also changed how the dispersant was applied: prior to Top Hat, a single wand applicator allowed dispersant entrainment into the side of the plume at the riser's end. Post-Top Hat the dispersant was applied through a multipronged

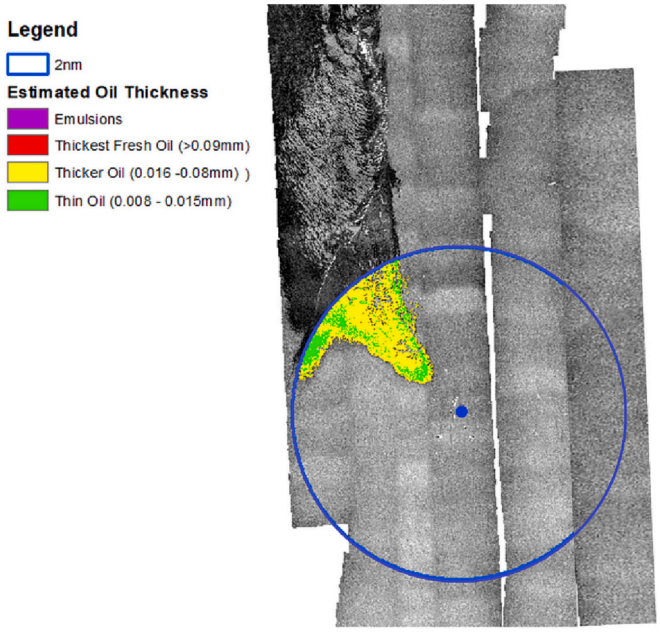

Fig. 4. Thermal IR image mosaic of the DWH source region from 23 May 2010 showing a typical, expanding oil plume (dark shades). Blue dot shows location of the wellhead and circle shows boundary of the 2 nm (3.7 km) radius study area, with oil classified for thickness. On this day the plume apex was displaced by 1.66 km to the northwest from the well location – the largest displacement recorded in the available image series. Due to the extreme displacement, this data set was not included in the correlation analysis. (For interpretation of the references to color in this figure legend, the reader is referred to the web version of this article.)

trident at the outer edge of the Top Hat. This is believed to have increased the volume of treated oil from 8.1 % to ~30 % (French-McCay et al., 2021). On a broader time scale, we found no significant changes in the SSDI rate vs. thick oil surface area relationship before and after Top Hat. The largest fresh thick oil area coverages (>20 % of study area) were observed before 15 May 2010 with no or minimal SSDI input and prior to Top Hat, but also during 7–9 June 2010 when the Top Hat installation was functioning. The lack of any obvious influence of the Top Hat operation on our data may be explained by the fact that the oil recovery volumes were not constant after installation. Maximum daily recovery was achieved between 17 June and 9 July, when up to 42 % of the estimated daily discharge was captured through Top Hat (Lehr et al., 2010). Of the 13 imaging data sets acquired after 6/4/2010 and used in the analysis, only 3 coincided with days that the oil recovery was at full operation, with the others coinciding with 10–25 % recovery rates.

It is important to note that our observations and analysis are limited to the SIMOPS area directly above the wellhead, and we do not make assertions about total surfaced oil volumes of the entire spill. An argument could be made that the SSDI effects caused a reduction of heavy surface oiling around the well site from rapidly rising large oil droplets, but potentially increased the number of surfacing smaller droplets further downfield, out of the study area. Modeling results by French-McCay et al. (2021) predicted that on average there was 9 % less oil floating on the surface during May–July because of the subsea dispersant applications. MacDonald et al. (2015) attempted to track changes in surfaced oil volume over the entire spill area using SAR satellite image series. They quantified the oil film thickness using a neural network-based algorithm which separates emulsified oil from all other oil thicknesses (Garcia-Pineda et al., 2013). MacDonald et al. (2015) assigned a thickness of 70 μm to the emulsion class and 1 μm to the non-emulsified oil class. Using these parameters to compute total surfaced oil volume, they found the area covered by oil of any thickness to have increased by 49 % between late May and mid-June, but the total volume to decrease by 21 %. They ascribe the changes to increased applications of dispersants and surface burning operations. They do not, however, consider the effects of the Top Hat recovery operation that was recovering a significant portion of the estimated daily discharge by mid-June. Thus any effects by SSDI on the overall spill footprint are unclear. Within the SIMOPS area, however, where ship-based operations were greatly concentrated, our results on floating oil, and Zhao et al.'s (2021) results on VOCs support the notion that SSDI significantly reduced the amount

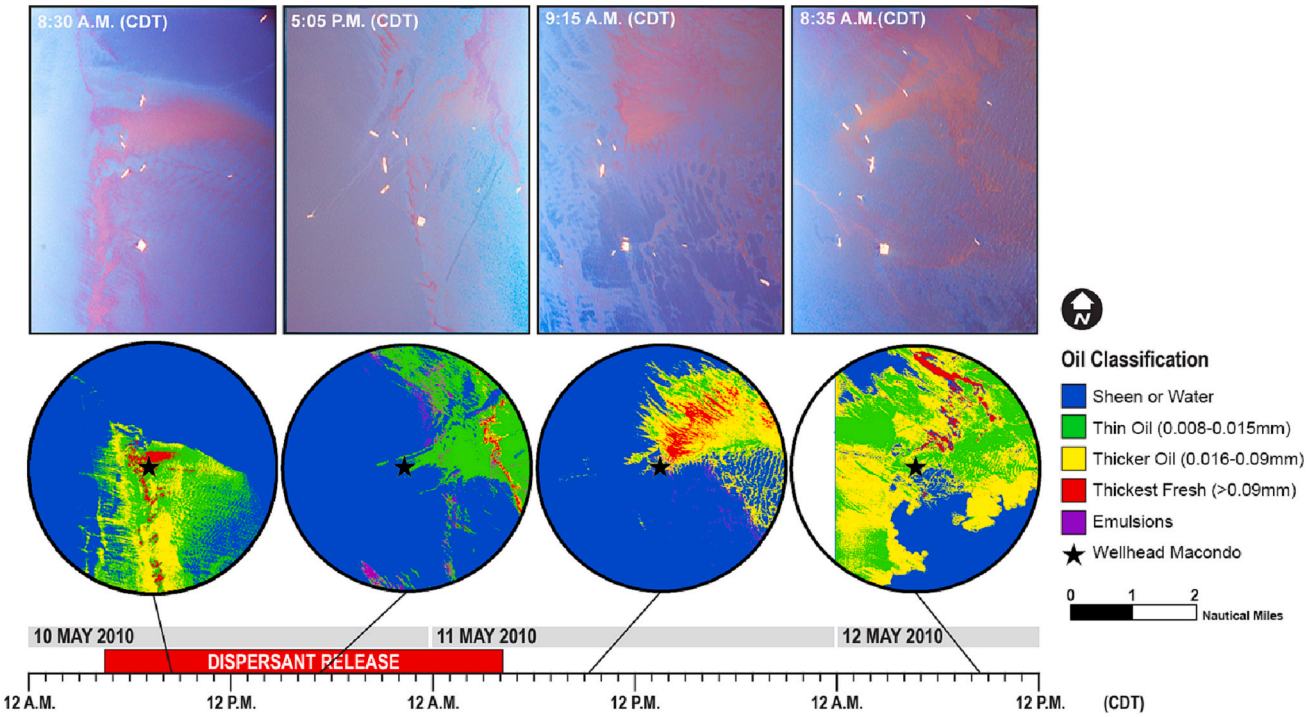

Fig. 5. SLR photos (top) and DMSC-derived surface oil thickness classifications related to the 10–11 May SSDI test timeline.

of oil reaching the surface.

CRediT authorship contribution statement

Jan Svejkovsky: Conceptualization, Methodology, Investigation, Analysis, Writing original draft and editing, Project supervision.
Mark Hess: Methodology, Investigation, Analysis.
Judd Muskat: Software, Analysis, Data visualization.
James White: Data curation, Data Visualization, Analysis.

Declaration of competing interest

The authors declare that they have no competing financial interests or personal relationships that could have appeared to influence the work reported in this paper.

Data availability

The data that has been used is confidential.

Acknowledgements

This project was supported by the American Petroleum Institute, Contract #114061. We thank our API member advisory committee for their valuable input to the research and manuscript.

References

Aman, Z., Paris, C.B., May, E., Johns, M., 2015. High-pressure visual experimental studies of oil-in-water dispersion droplet size. Chem. Eng. Sci. 127, 392–400. https://doi.org/10.1016/j.ces.2015.01.058.

Aprin, L., Heymes, F., Lauret, P., Slangen, P., 2015. Experimental characterization of the influence of dispersant addition on rising oil droplets in water column. Chem. Eng. Trans. 43, 2287–2292. https://doi.org/10.3303/CET1543382. hal-02014363.

Bracco, A., Paris, C.B., Esbaugh, A.J., Frasier, K., Joye, S.B., Liu, G., Polzin, K.L., Vaz, A. C., 2020. Transport, fate and impacts of the deep plume of petroleum hydrocarbons formed during the Macondo blowout. Front. Mar. Sci. 7, 764. https://doi.org/10.3389/fmars.2020.542147.

Brandvik, P.J., Johansen, O., Leirvik, F., Farooq, U., Daling, P.S., 2013. Droplet breakup in sub-surface oil releases—part 1: experimental study of droplet breakup and effectiveness of dispersant injection. Mar. Pollut. Bull. 73, 319–326. https://doi.org/10.1016/j.marpolbul.2013.05.020.

Brandvik, J., Johansen, O., Leirvik, F., Krause, D.F., Daling, P.S., 2018. Subsea dispersants injection (SSDI), effectiveness of different dispersant injection techniques – an experimental approach. Mar. Pollut. Bull. 136, 385–393. https://doi.org/10.1016/j.marpolbul.2018.09.021.

French-McCay, D.P., Jayko, K., Li, Z., Spaulding, M.L., Crowley, D., Medelsohn, D., Horn, M., Isaji, T., Kim, Y.H., Fontenault, J., Rowe, J.J., 2021. Oil fate and mass balance for Deepwater Horizon oil spill. Mar. Pollut. Bull. 171, 112681 https://doi.org/10.1016/j.marpolbul.2021.112681.

Garcia-Pineda, O., MacDonald, I., Hu, C., Svejkovsky, J., Hess, M., Dukhovskoy, D., Morey, S.L., 2013. Detection of floating oil anomalies from the Deepwater Horizon oil spill with synthetic aperture radar. Oceanography 26 (2), 124–137. https://doi.org/10.5670/oceanog.2013.38.

Gros, J., Socolofsky, S.A., Dissanayake, A.L., Jun, I., Zhao, L., Boufadel, M.C., Reddy, C. M., Arey, J.S., 2017. Petroleum dynamics in the sea and influence of subsea dispersant injection during Deepwater Horizon. Proc. Natl. Acad. Sci. 114 (38), 10065–10070. https://doi.org/10.1073/pnas.1612518114.

Gulf Stream Initiative, 2018. https://data.gulfresearchinitiative.org/data/BP.x750.000:0018. Last accessed 2/16/2023.

Johansen, O., 2003. Development and verification of deep-water blowout models. Mar. Pollut. Bull. 47 (9–12), 360–368. https://doi.org/10.1016/s0025-326x(03)00202-9.

Johansen, O., Rye, H., Cooper, C., 2003. DeepSpill – field study of a simulated oil and gas blowout in deep water. Spill Sci. Technol. Bull. 8 (5–6), 433–443. https://doi.org/10.1016/S1353-2561(02)00123-8.

Johansen, O., Brandvik, P.J., Farooq, U., 2013. Droplet breakup in sub-surface oil Releases—Part 2: predictions of droplet size distributions with and without injection of chemical dispersants. Mar. Pollut. Bull. 73, 327–335.

Lehr, W., Bristol, S., Possolo, A., et al., 2010. Oil Budget Calculator, Deepwater Horizon, Technical Documentation. A Report to the National Incident Command. The Federal Interagency Solutions Group, Oil Budget Calculator Science and Engineering Team. http://www.restorethegulf.gov/sites/default/files/documents/pdf/OilBudgetCalc_Full_HQ-Print_111110.pdf. November 2010. (Accessed on 6 February, 2023).

Lindo-Atichati, D., Paris, C.B., Le Henaff, M., Schedler, M., Juarez, A.G.Valladares, Müller, R., 2016. Simulating the effects of droplet size, high-pressure biodegradation, and variable flow rate on the subsea evolution of deep plumes from the Macondo blowout. Deep Sea Res. Part II: Top. Stud. Oceanogr. 0 https://doi.org/10.1016/j.dsr2.2014.01.011.

MacDonald, I.R., Garcia-Pineda, O., Beet, A., DaneshgarAsl, S., Feng, L., Graettinger, G., French-McCay, D., Holmes, J., Hu, C., Huffer, F., Leifer, I., Muller-Karger, F., Solow, A., Silva, M., Swayze, G., 2015. Natural and unnatural oil slicks in the Gulf of Mexico. J. Geophys. Res. Oceans 120 (8), 364–368. https://doi.org/10.1002/2015JC011062.

Malone, K., Pesch, S., Schluüter, M., Krause, D., 2018. Oil droplet size distributions in deep-sea blowouts: influence of pressure and dissolved gases. Environ. Sci. Technol. 52, 6326–6333. https://doi.org/10.1021/acs.est.8b00587.

NOAA, 2015. https://www.diver.orr.noaa.gov/documents/20233/39182/BP+Dispersant+Volumes+Logs.zip/6c33d118-b946-584b-3ece-d7b2e6b3a467. Last accessed 2/16/2023.

Paris, C.B., Henaff, M.L., Aman, Z.M., Subramaniam, A., Helgers, J., Wang, D.-P., Kourafalou, V.H., Srinivasan, A., 2012. Evolution of the Macondo well blowout: simulating the effects of the circulation and synthetic dispersants on the subsea oil transport. Environ. Sci. Technol. 46, 13293–13302. https://doi.org/10.1021/es303197h.

Paris, C.B., Berenshtein, I., Trillo, M.L., Faillettaz, R., Olascoaga, M.J., Aman, Z.M., Schlüter, M., Joye, S.B., 2018. BP gulf science data reveals ineffectual subsea dispersant injection for the Macondo blowout. Front. Mar. Sci. 5, 389. https://doi.org/10.3389/fmars.2018.00389.

Peterson, C.H., Anderson, S., Cherr, G., Ambrose, R., Anghera, S., Bay, S., Blum, M., Condon, Dean, T., Graham, M., Guzy, M., Hampton, S., Joye, S., Lambrinos, J., Meffert, D., Powers, S., Somasundaran, P., Spies, R., Taylor, C., Tjeerdema, R., Adams, E., Mate, B., 2012. A tale of two spills: novel science and policy implications of an emerging new oil spill model. BioScience 62 (5), 461–469. https://doi.org/10.1525/bio.2012.62.5.7.

Ryerson, T.B., Camilli, R., Kessler, J.D., Kujawinski, E.B., Reddy, C.M., Valentine, D.L., Atlas, E., Blake, D.R., De Gouw, J., Meinardi, S., Parrish, D.D., Peischl, J., Seewald, J. S., Warneke, C., 2012. Chemical data quantify Deepwater horizon hydrocarbon flow rate and environmental distribution. Proc. Natl. Acad. Sci. 109 (50), 20246–20253. https://doi.org/10.1073/pnas.1110564109.

Socolofsky, S.A., Adams, E.E., Sherwood, C.R., 2011. Formation dynamics of subsurface hydrocarbon intrusions following the Deepwater Horizon blowout. Geophys. Res. Lett. 38, L09602 https://doi.org/10.1029/2011GL047174.

Socolofsky, S.A., Adams, E.E., Boufadel, M.C., Aman, Z.M., Johansen, Ø., Konkel, W.J., Lindo, D., Madsen, M.N., North, E.W., Paris, C.B., Rasmussen, D., Reed, M., Rønningen, P., Sim, L.H., Uhrenholdt, T., Anderson, K.G., Cooper, C., Nedwed, T.J., 2015. Intercomparison of oil spill prediction models for accidental blowout scenarios with and without subsea chemical dispersant injection. Mar. Pollut. Bull. 96 (1–2), 110–126. https://doi.org/10.1016/j.marpolbul.2015.05.039.

Spaulding, M., Li, Z., Mendelsohn, D., Crowley, D., French-McCay, D., Bird, A., 2017. Application of an integrated blowout model system, OILMAP DEEP, to the Deepwater horizon (DWH) spill. Mar. Pollut. Bull. 120, 37–50. https://doi.org/10.1016/j.marpolbul.2017.04.043.

Spier, C., Stringfellow, W.T., Hazen, T.C., Conrad, M., 2013. Distribution of hydrocarbons released during the 2010 MC252 oil spill in deep offshore waters. Environ. Pollut. 173, 224–230. https://doi.org/10.1016/j.envpol.2012. 10.019.

Svejkovsky, J., Muskat, J., 2006. Real-time detection of oil slick thickness patterns with a portable multispectral sensor. In: Final Report for U. S. Minerals Management Service Contract 0105CT39144, 37 p.

Svejkovsky, J., Muskat, J., Mullin, J., 2008. Mapping Oil Spill Thickness with a Portable Multispectral Aerial Imager. Proc. International Oil Spill Conference 2008, 4-8 May, 2008, Savannah, Georgia unpaginated USB flash drive.

Svejkovsky, J., Muskat, J., 2009. Development of a portable multispectral aerial sensor for real-time oil spill thickness mapping in coastal and offshore waters. In: Final Report for U. S. Minerals Management Service Contract M07PC13205, 33p.

Svejkovsky, J., Muskat, J., Mullin, J., 2009. Adding a multispectral aerial system to the oil spill response arsenal. Sea Technology 50 (8), 17–22.

Svejkovsky, J., Hess, M., 2012. Expanding the utility of remote sensing data for oil spill response. Photogramm. Eng. Remote Sens. 78 (10), 1011–1014.

Svejkovsky, J., Lehr, W., Muskat, J., Graettinger, G., Mullin, J., 2012. Operational utilization of aerial multispectral remote sensing during oil spill response: lessons learned during the Deepwater Horizon (MC-252) spill. Photogramm. Eng. Remote. Sens. 78 (10), 1089–1102. https://doi.org/10.14358/PERS.78.10.1089.

Svejkovsky, J., Hess, M., Muskat, J., Nedwed, T.J., McCall, J., Garcia, O., 2016. Characterization of surface oil thickness distribution patterns observed during the Deepwater horizon (MC-252) oil spill with aerial and satellite remote sensing. Mar. Pollut. Bull. 110 (1), 162–176. https://doi.org/10.1016/j.marpolbul.2016.06.066.

Zhao, L., Mitchell, D., Prince, R., Hayward Walker, A., Arey, J., Nedwed, T., 2021. Deepwater horizon 2010: subsea dispersants protected responders from VOC exposure. Mar. Pollut. Bull. 173 (B), 113034 https://doi.org/10.1016/j.marpolbul.2021.113034.